Discrete wavelet transform and energy eigen value for rotor bars fault detection in variable speed field-oriented control of induction motor drive

Tarek Ameid, Arezki Menacer, Hicham Talhaoui, Youness Azzoug

Discrete wavelet transform and energy eigen value for rotor bars fault detection in variable speed field-oriented control of induction motor drive

Tarek Ameid[a,*], Arezki Menacer[a], Hicham Talhaoui[a,b], Youness Azzoug[a]

[a] LGEB Laboratory, Electrical Engineering Department, Biskra University, Algeria
[b] University of Bordj Bou Arreridj, Algeria

ARTICLE INFO

Keywords:
Induction motor
Vector control
Fault diagnosis
Broken rotor bars
Discrete wavelet transform
dSpace 1104

ABSTRACT

This paper presents a methodology for the broken rotor bars fault detection is considered when the rotor speed varies continuously and the induction machine is controlled by Field-Oriented Control (FOC). The rotor fault detection is obtained by analyzing a several mechanical and electrical quantities (i.e., rotor speed, stator phase current and output signal of the speed regulator) by the Discrete Wavelet Transform (DWT) in variable speed drives. The severity of the fault is obtained by stored energy calculation for active power signal. Hence, it can be a useful solution as fault indicator. The FOC is implemented in order to preserve a good performance speed control; to compensate the broken rotor bars effect in the mechanical speed and to ensure the operation continuity and to investigate the fault effect in the variable speed. The effectiveness of the technique is evaluated in simulation and in a real-time implementation by using Matlab/Simulink with the real-time interface (RTI) based on dSpace 1104 board.

1. Introduction

In industry, drive applications require high performances, the squirrel-cage induction motor (IM) takes an important place due to its rigidity, and works more efficiently compared to the wounded rotor. In addition, it adjusts to several service applications, where the speed should closely follow a trajectory specified reference that is independent of any external load disturbance. The operation modes of the IM are vulnerable to a variety of unwanted conditions, which make it susceptible to different types of defaults. In this respect, these faults in the machine can be classified into two categories: on the one hand, External, such as: overload, poor mounting, the voltage and the environmental phenomena. On the other hand, Internal, such as: inter-turn short circuit [1,2], eccentricity of the rotor [3,4] and broken rotor bars [5,6]. The broken rotor bars fault causes fluctuation and decreases torque's amplitude; therefore, more fluctuation and mechanical vibrations can be produced, and then these problems can lead to the damage of the machine. Ultimately, the rotor bars fault effect becomes more obvious by the increase of the broken bars number, especially, in the open-loop drives [7]. To avoid such problems, the fault diagnosis and detection process become highly necessary step to protect this type of electrical components [8].

The purpose of the field-oriented control is to have good performance flux and torque decoupled control, this technique has led to a radical change in control of the IM [9]. The recommended machine model for closed-loop FOC design takes into account the effective geometry of the rotor based on multi-winding model for diagnosis purpose considering the broken rotor bars fault [10].

In recent years, several techniques for the fault detection have been proposed in the literature; they focused on the diversity of the encountered problems, and have made it a challenging topic for many researchers. Furthermore, it is usually known that the developed techniques for IMs diagnosis in open-loop drives are not so effective when the motor's control structure becomes more complex, particularly, the closed-loop vector controlled motors [11–14].

The use of signals approach for diagnosis has a great importance for the broken rotor bars detection. It's necessary to employ different analysis to interpret the acquired signals for the detection process, such as stator voltage, current, speed, temperature, and vibration signals [13,14]. The monitoring and diagnosis based on motor current signature analysis (MCSA) are widespread used methods, whereas, they present many advantages like requiring only one current sensor per machine, and is based on straightforward signal processing such as Fast Fourier Transforms (FFT) [15,16]. The FFT analysis method has been proved to be a good technique for fixed frequency supply, such as the connected machines to the electrical grid (steady-state), where it is used to determine the spectral signatures by investigating components around the fundamental frequency [17]. However, the effectiveness

and accuracy of the FFT are affected by the amount of time domain data. In addition this can be more affective in cases of inconstant load or speed, since both of them make a variation on the motor slip or time-frequency. Therefore, this assumption may be considered as a limitation of this approach and the FFT analysis cannot be applied by consequence. For this reason, the wavelet decompositions becomes our main focus in this paper which will be proposed in order to overcome the aforementioned difficulties [18–21].

The wavelet transform is a window technique with a variable size. It is used in order to improve the stator phase current analysis in steady and transient states. The wavelet transform is a new description of spectral decomposition via the scaling concept. Wavelet theory offers a unified framework for many techniques, which have been developed for different applications in the field of signal-processing. Moreover, it can provide information in both of time and frequency domains [22,23].

In Ref. [24], the authors present a method for the broken rotor bar fault detection based on discrete wavelet coefficients, when the induction motor operates with load variation. Others [25] use the DWT for the current space vector magnitude or the instantaneous magnitude of the stator phase current analysis, the energy associated to the rotor fault in the frequency bandwidth is computed, this energy allows to evaluate the fault severity without any slip estimation. The DWT is used in Refs. [18,26] for the analysis of stator current to detect the rotor bars fault in steady and start-up transient states, the calculation of the energy Eigenvalue of the stator current signal proves its importance as a good fault severity indicator. In most cases, the diagnostic methods are used for open-loop machine operation. However, in closed-loop drives, the control-loop masks and compensates the fault effect [10]. As a consequence, they cause a difficulty in fault detection using stator current analysis. Some attempts can be found in literature which uses other quantities for fault analysis. For instance, in Refs. [27,28], d (direct) and q (quadratic) current axis components have been used for broken rotor bars detection in closed-loop drive. Nevertheless in case of variable speed drive, the continuous speed variation between two reference values causes a non-stationary state in the signals and confusion in the DWT spectrum, consequently a more difficulties in the fault diagnosis process.

The main objectives of this paper are the diagnosis of the broken rotor bars fault and the evaluation of the fault severity when the IM operates in closed-loop drive with continuous speed change. The FOC control strategy is presented to preserve a high performance decoupled control. The used method for the fault detection is DWT analysis which will be applied to output signal of the speed regulator and stator phase current. The choice of this technique has been done to ensure a good diagnosis during the continual variation of speed. The evaluation of the stored energy in each level of the active power energy allows both, to evaluate the fault severity (break or fissure), and to distinguish between fault and normal variation.

The effectiveness of the control scheme with diagnosis method will be investigated in simulation and experimentation using the Matlab/Simulink software and hardware implementation using Real-Time interface (RTI) environment based on dSpace 1104 board. The realization of the control strategy is done by Digital Signal Processor with graphical programming platform (Matlab/Simulink/Control Desk). The simulation and experimental validation has shown a good dynamic control under rotor bars fault, wherein, the same signatures of the fault are proved in both results.

This paper is structured as follows: Section 2 presents the dynamic modeling of the IM taking into account the rotor bars fault. Section 3 describes the vector controlled IM. In section 4, the discrete wavelet transforms method is proposed. Section 5 illustrates and discusses the simulation results of the proposed control technique with diagnosis method. Then, the experimental validation is presented in Section 6.

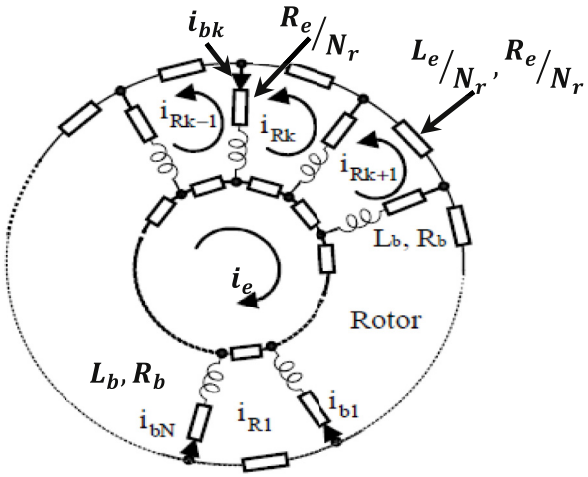

Fig. 1. Rotor cage equivalent circuit of induction machine.

2. Modeling of the induction motor with taking into account the rotor bars fault

The development of the reduced model which is dedicated for closed-loop control is inspired by the multi-winding model of the induction machine. This proposed model takes into account the rotor geometry which is considered as a squirrel-cage. The modeling is based on the equivalent scheme of the rotor which is shown in Fig. 1. It can be noticed that each bar of the rotor cage is represented by a resistance R_b, in series, with a leakage inductance L_b. The short-circuit ring portion between the two bars, as well, is represented by a resistance R_e in series with a leakage inductance L_e. A mesh is composed of two bars and two portions, hence, the cage is modeled by q number of meshes where each mesh represents one of the two rings of the short circuit, which are located on the rotor periphery. Therefore, with N_r number of bars, the cage contains $2N_r$ nodes and $3N_r$ branches based on the theory of electrical circuits. As a result, the number of independent currents in the cage is: $3N_r - (2N_r - 1) = N_r + 1$ [29,30].

The modeling steps are presented in details in Refs. [14] and [15] in order to highlight the effect of the broken rotor bar fault. This model presents a difficulty in the control implementation, due to the big number of equations. To transform the system in N_r phases into *(d, q)* system, the extended Park's transformation of the rotor will be applied.

The system is put in canonical form:

$$[L]\frac{d[I]}{dt} = [V] - [R][I] \tag{1}$$

where:

$$[L] = \begin{bmatrix} L_{sc} & 0 & -\frac{N_r}{2}M_{sr} & 0 & 0 \\ 0 & L_{sc} & 0 & -\frac{N_r}{2}M_{sr} & 0 \\ -\frac{3}{2}M_{sr} & 0 & L_{rc} & 0 & 0 \\ 0 & -\frac{3}{2}M_{sr} & 0 & L_{rc} & 0 \\ 0 & 0 & 0 & 0 & L_e \end{bmatrix}; \quad [R]$$

$$= \begin{bmatrix} R_s & -\omega_r L_{sc} & 0 & \frac{N_r}{2}\omega_r M_{sr} & 0 \\ \omega_r L_{sc} & R_s & -\frac{N_r}{2}\omega_r M_{sr} & 0 & 0 \\ 0 & 0 & [R_{rdd} & R_{rdq}] & 0 \\ 0 & 0 & [R_{rqd} & R_{rqq}] & 0 \\ 0 & 0 & 0 & 0 & R_e \end{bmatrix};$$

As:

The total cyclic inductance of a stator phase which is given by the following equation:

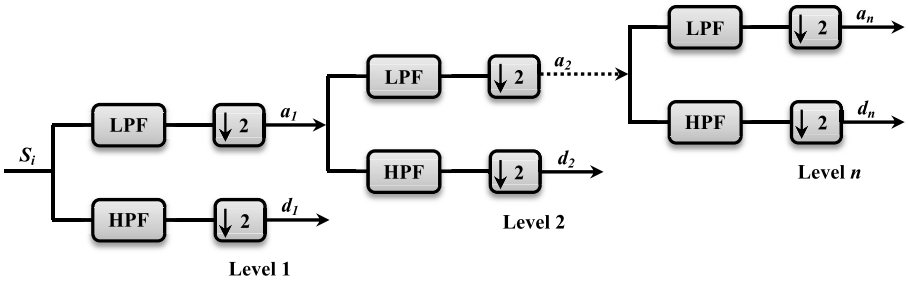

Fig. 2. DWT decomposition process at level n.

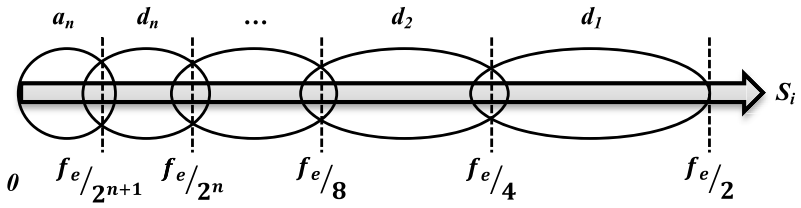

Fig. 3. Multi-level decomposition n.

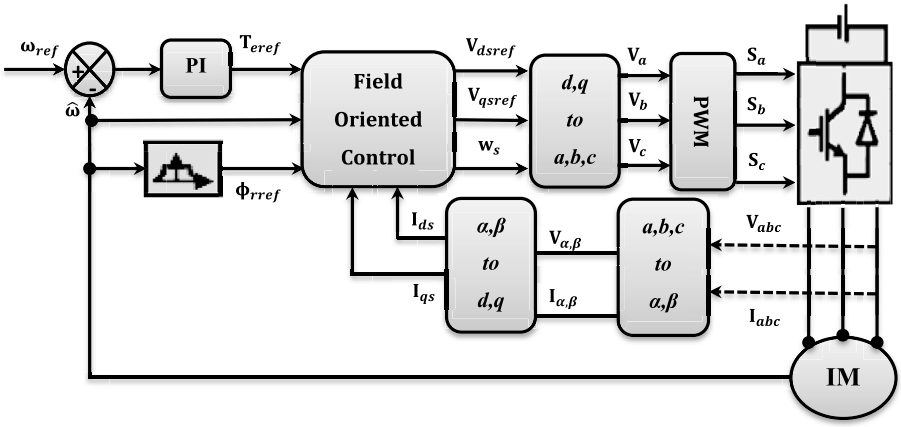

Fig. 4. Block diagram of vector control of the IM with rotor fault.

$$L_{cs} = L_{sp} + L_{sf}$$

The magnetizing inductance is: $L_{sp} = 4\mu_0 \frac{N_s^2 r.l}{e.p^2\pi}$.

The mutual inductance of the stator/rotor is: $M_{sr} = (4/\pi)(\mu_0/e.\ p^2)N_s.\ r.\ l \sin(a/2)$.

The total cyclic inductance of the rotor is calculated by:

$$L_{rc} = L_{rp} - M_{rr} + 2\frac{L_e}{N_r} + 2L_e(1-\cos\alpha) \tag{2}$$

where:

The rotor mesh inductance can be calculated by the following equation: $L_{rp} = \left(\frac{N_r - 1}{N_r^2}\right)\frac{\mu_0}{e}2\pi.\ r.\ l$

The mutual inductance between non adjacent rotor meshes is defined by: $M_{rr} = -\frac{1}{N_r^2}\frac{\mu_0}{e}2\pi.\ r.\ l$

The electrical angle of two adjacent rotor meshes: $\alpha = p\frac{2\pi}{N_r}$

The four matrices, taking into account the broken rotor bars fault, can be expressed by:

$$\begin{cases} R_{rdd,rqq} = R_r + \frac{2}{N_r}(1-\cos\alpha)\sum_k R_{bfk}.(1 \pm \cos(2k-1).\alpha) \\ R_{rdq,rqd} = -\frac{2}{N_r}(1-\cos\alpha)\sum_k R_{bfk}.\sin(2k-1).\alpha \end{cases} \tag{3}$$

In this expression, the summation is applied to all bars with fault. R_{bfk} is the increased resistance of the bar index k from its initial value before the fault.

3. Vector control based on the reduced model of IM

The Field-oriented control of the IM has been developed to allow a speed variation over a wide range. It separates the stator currents of IM into flux torque components in the *(d, q)* coordinate reference frame. The model system Eq. (1) is a heavily coupled, multivariable and nonlinear system. Those properties complicate the control design of the IM. The rotor flux-oriented coordinate is applied in order to simplify the model of the IM, where the rotor flux and the electromagnetic torque are aligned to the direct axis *(d)* and quadratic axis *(q)* respectively. In this coordinate system the rotor flux is assumed as [10,31].

$$\begin{cases} \phi_{dr} = \phi_r \\ \phi_{qr} = 0 \end{cases} \tag{4}$$

The electromagnetic torque of IM is defined by:

$$T_e = -\frac{3}{4}p\frac{N_r.\ M_{sr}}{L_{rc}}(\phi_{dr} i_{qs} - \phi_{qr} i_{ds}) \tag{5}$$

While the quadratic flux is: $\phi_{qr} = 0$, the electromagnetic torque expression becomes:

$$T_e = -\frac{3}{4}p\frac{N_r.\ M_{sr}}{L_{rc}}\phi_{dr} i_{qs} = K.\ \phi_{dr} i_{qs} \tag{6}$$

where:

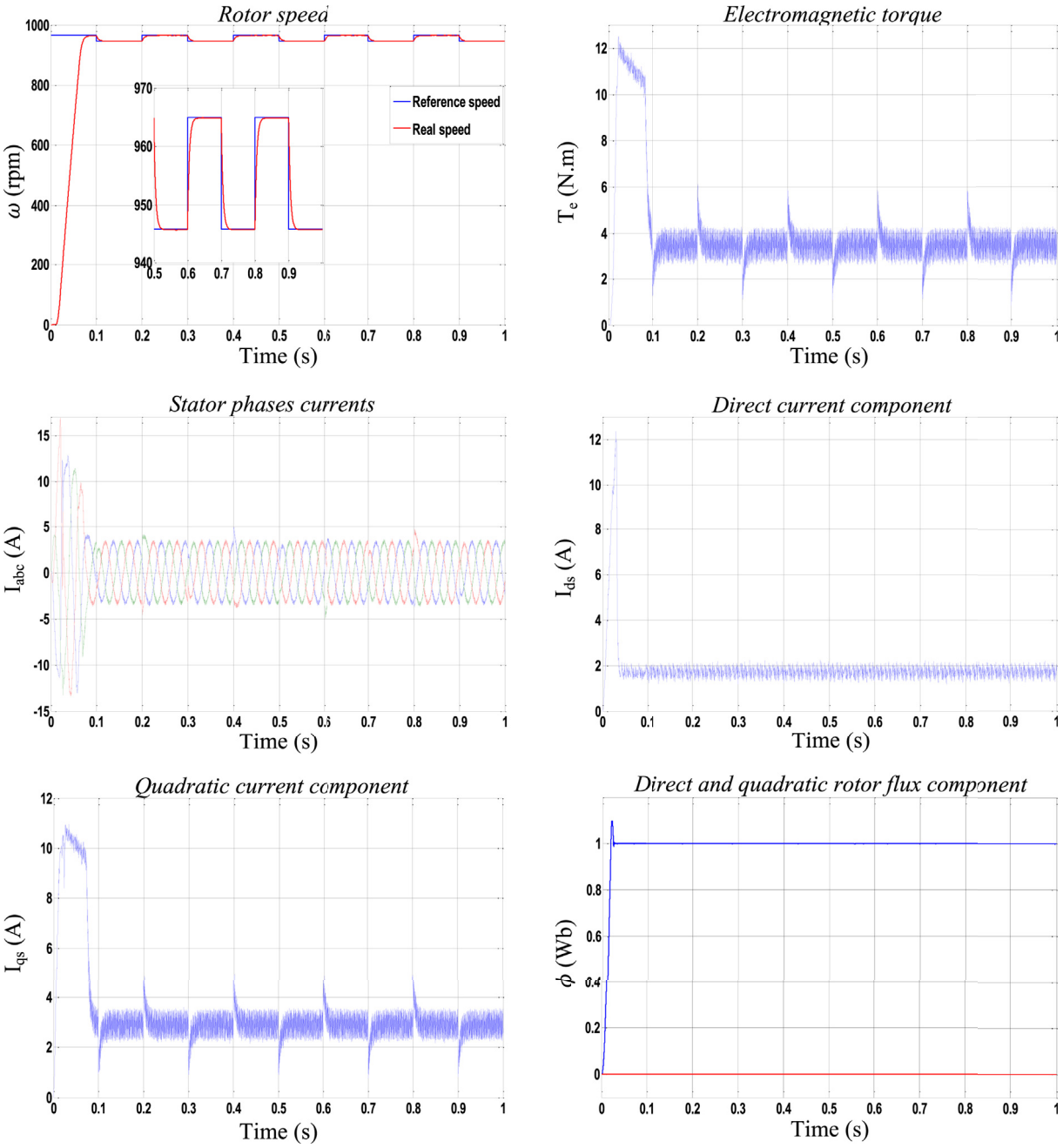

Fig. 5. Electrical and mechanical characteristic of the vector controlled IM in healthy state.

$$K = -\frac{3}{4}p\frac{N_r.\,M_{sr}}{L_{rc}}$$

The rotor flux components are expressed in the stator reference as:

$$\begin{cases} \phi_{ds} = L_{sc}.\,i_{ds} - \frac{N_r}{2}M_{sr}.\,i_{dr} \\ \phi_{qs} = L_{sc}.\,i_{qs} - \frac{N_r}{2}M_{sr}.\,i_{qr} \\ \phi_{dr} = -\frac{3}{2}M_{sr}.\,i_{ds} + L_{rc}.\,i_{dr} \\ \phi_{qr} = -\frac{3}{2}M_{sr}.\,i_{qs} + L_{rc}.\,i_{qr} \end{cases} \tag{7}$$

By applying the field orientation, the current components become:

$$\begin{cases} i_{ds} = -\frac{2}{3}\left(\frac{\phi_{dr}(1+T_r.s)}{M_{sr}}\right) \\ i_{qs} = \frac{T_e}{K.\phi_{dr}} \end{cases} \tag{8}$$

where:

$T_r = L_{rc}/R_r$: Rotor time constant.

From using Eq. (1) and Eq. (7), the model for vector control design of IM is shown in Eq. (9), with the stator current, rotor flux and ring current are taken as state variables:

$$\begin{cases} \dot{x}(t) = Ax(t) + Bu(t) \\ y(t) = Cx(t) \end{cases} \tag{9}$$

As.

$x^T = [i_{ds} \;\; i_{qs} \;\; \phi_{dr} \;\; \phi_{qr} \;\; i_e]$; $u^T = [V_{ds} \;\; V_{qs}]$; $y^T = [i_{ds} \;\; i_{qs}]$;

$$A = \begin{bmatrix} -a_1 - a_2R_{rdd} & \omega_r - a_2R_{rdq} & -a_3R_{rdd} & -a_4\omega_r - a_3R_{rdq} & 0 \\ -\omega_r - a_2R_{rqd} & -a_1 - a_2R_{rqq} & a_4\omega_r - a_3R_{rqd} & -a_3R_{rqq} & 0 \\ -a_5R_{rdd} & -a_5R_{rdq} & -a_6R_{rdd} & -a_6R_{rdq} & 0 \\ -a_5R_{rqd} & -a_5R_{rqq} & -a_6R_{rqd} & -a_6R_{rqq} & 0 \\ 0 & 0 & 0 & 0 & -a_7 \end{bmatrix};$$

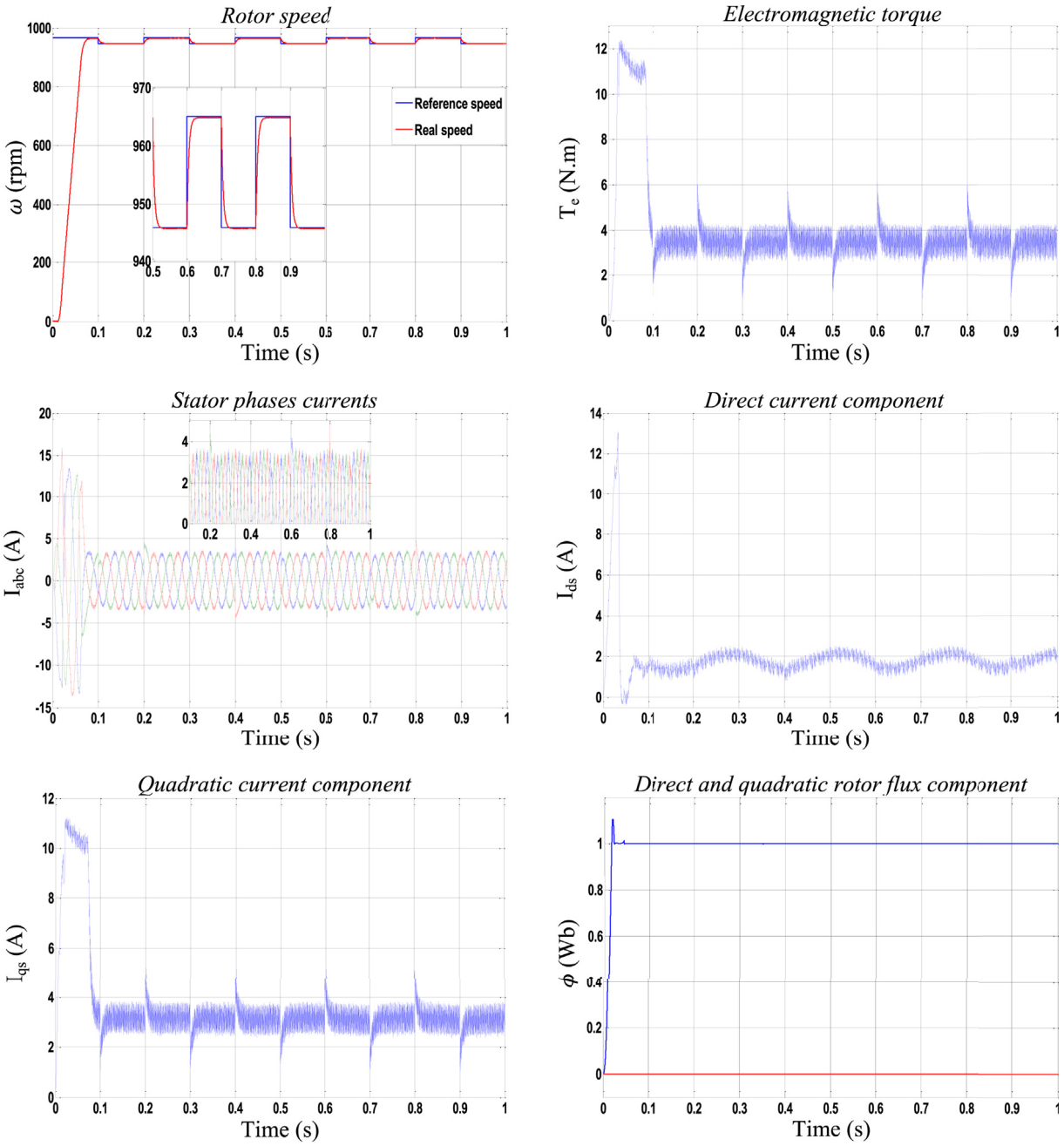

Fig. 6. Electrical and mechanical characteristic of the vector controlled IM in faulty state.

Table 1
Frequency Levels of Wavelet Coefficients in simulation tests.

Level	Frequency band
d_1	2500–5000 Hz
d_2	1250–2500 Hz
d_3	625–1250 Hz
d_4	312.5–625 Hz
d_5	156.25–312.5 Hz
d_6	78.12–156.25 Hz
d_7	39.06–78.12 Hz
d_8	19.53–39.06 Hz
d_9	9.76–19.53 Hz
d_{10}	4.88–9.76 Hz
a_{10}	0–4.88 Hz

$$B = \begin{bmatrix} a_8 & 0 & 0 & 0 & 0 \\ 0 & a_8 & 0 & 0 & 0 \end{bmatrix}^T;\ C = \begin{bmatrix} 1 & 0 & 0 & 0 & 0 \\ 0 & 1 & 0 & 0 & 0 \end{bmatrix};$$

$$a_1 = \frac{R_s}{\sigma L_{sc}},\ a_2 = \frac{3M_{sr}^2.\ N_r}{4L_{sc}.\ L_{rc}^2.\ \sigma},\ a_3 = \frac{M_{sr}.\ N_r}{2L_{sc}.\ L_{rc}^2.\ \sigma},\ a_4 = \frac{M_{sr}.\ N_r}{2L_{sc}.\ L_{rc}.\ \sigma},\ a_5 = \frac{3M_{sr}}{2L_{rc}},\ a_6 = \frac{1}{L_{rc}},\ a_7 = \frac{R_e}{L_e},\ a_8 = \frac{1}{\sigma L_{sc}},\ \sigma = 1 - \left(\frac{3M_{sr}^2.\ N_r}{4L_{sc}.\ L_{rc}}\right)$$

4. Fault diagnosis of IM using discrete wavelet transform (DWT)

The application of conventional signal processing methods such as Fast Fourier Transform FFT in fault diagnosis, does not always give a good performance because of to the accuracy and the large sample size of signals, which requires a space memory. Furthermore, they have a fixed length of the window and they cannot be used in transient state

Table 2
Frequencies of the stator current and the output signal of the speed regulator with fault in simulation tests.

stator phase current I_a spectrum					quadratic current I_{qs} spectrum		
$s = 0.1145$	$(1\text{-}2s)f_s$	$(1\text{-}4s)f_s$	$(1+2s)f_s$	$(1+4s)f_s$	$s = 0.1145$	$2sf$	$4sf$
$f_{calculated}$ (Hz)	13.790	9.694	21.983	26.079	$f_{calculated}$ (Hz)	4.096	8.192

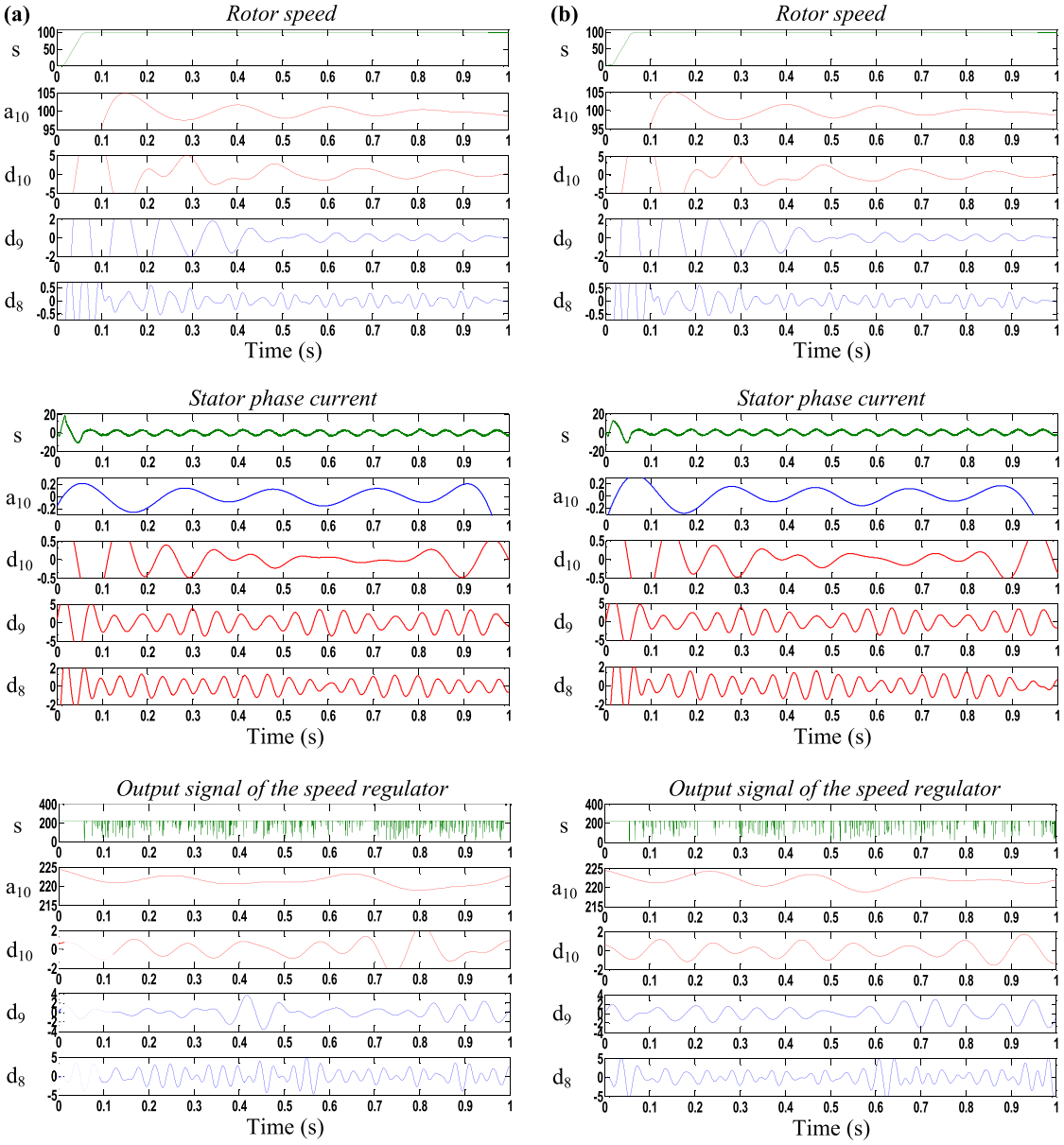

Fig. 7. DWT of the rotor speed, the stator phase current and the output signal of the speed regulator.

phenomena like the IM operates in the closed-loop drive with speed variation.

The wavelet transform is a similar tool to the Fourier transform; the difference is that the former decomposes the signal into a set of scaled and translated versions of a mother wavelet instead of using sine waves of different frequencies as the Fourier transform. The main advantage of this method is that flexibility in descripting the non-stationary states signals. Wavelet transforms is considered as an important aspect in speed and/or variable load, in this context, it is quite comparable to the Fourier analysis. However, wavelets are largely oscillating functions that are rapidly damped, unlike the sinusoidal functions of Fourier analysis [32,33].

The wavelet is divided into two categories: continuous and discrete, designate as a mathematical tool. In Continuous Wavelets Transform (CWT), the signal is multiplied by a function with the wavelet and the transform is calculated separately for different segments of the time-domain signal. The Discrete Wavelet Transform (DWT) also has the same main idea as the (CWT), however, it is developed mainly for the processing of sampled signals. In addition, DWT calculation is close to the idea of quick filter bench and it is easy to be implemented. Still this does not prevent the application of the continuous wavelet transform for analyzing the sampled signals [18,26].

The decomposition of the signal in multi-resolution is obtained by filters of different cut-off frequencies; they are used to analyze the

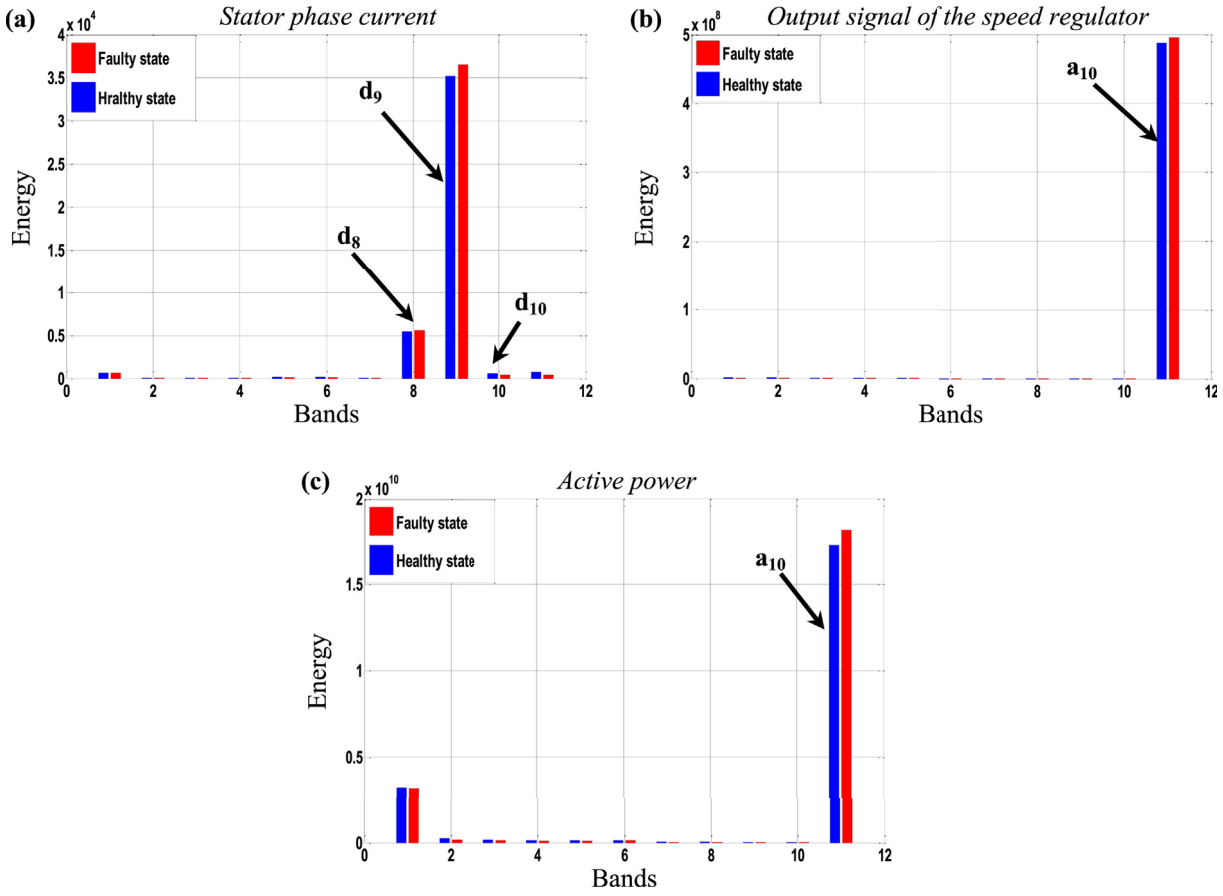

Fig. 8. Energy value in the simulation results for various levels (a) stator phase current, (b) output signal of the speed regulator and (c) active power.

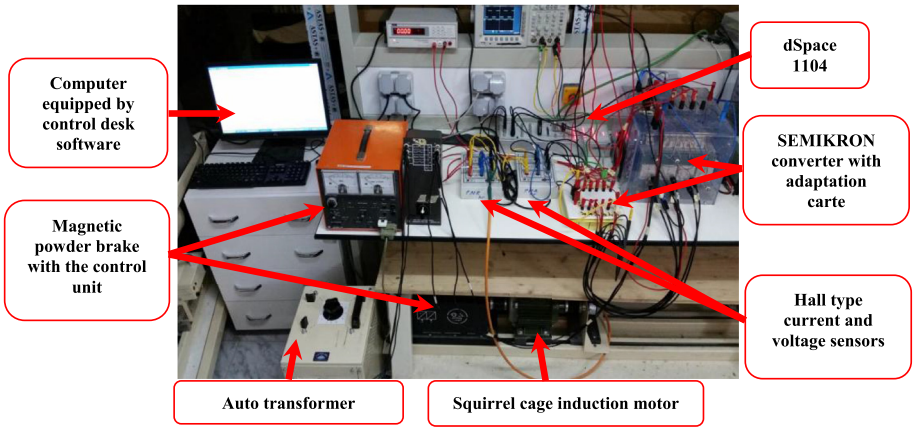

Fig. 9. Experimental test bench.

signal at different scales. The signal is passed both, through a series of high-pass filters H (details) to analyze the high frequencies, and through a series of low-pass filters L (approximations) to analyze the low frequencies as shown in Fig. 2, where it can see the detail and approximation signals reflect the time evolution of the associated frequency components of the original signal S_i, which are contained within their associated frequency band [34].

For decomposition process by the wavelet at level n (Fig. 2), the decomposition level of the first signal contains two coefficients, where a_1 is the approximate version and d_1 is the detailed representation. These coefficients can be calculated by the following expressions:

$$\begin{cases} a_1 = \sum_k^n L(k-2n)S_i(k) \\ d_1 = \sum_k^n H(k-2n)S_i(k) \end{cases} \quad (10)$$

The next decomposition level is based on the a_1 coefficient. Therefore, the new coefficients can be expressed as:

$$\begin{cases} a_2 = \sum_k^n L(k-2n)a_1(k) \\ d_2 = \sum_k^n H(k-2n)a_1(k) \end{cases} \quad (11)$$

The computing of higher-level decompositions is done in a similar ways. After the decomposition process, the original signal S_i can be reconstructed again [4] as shown in Fig. 3. This recursive process is given by:

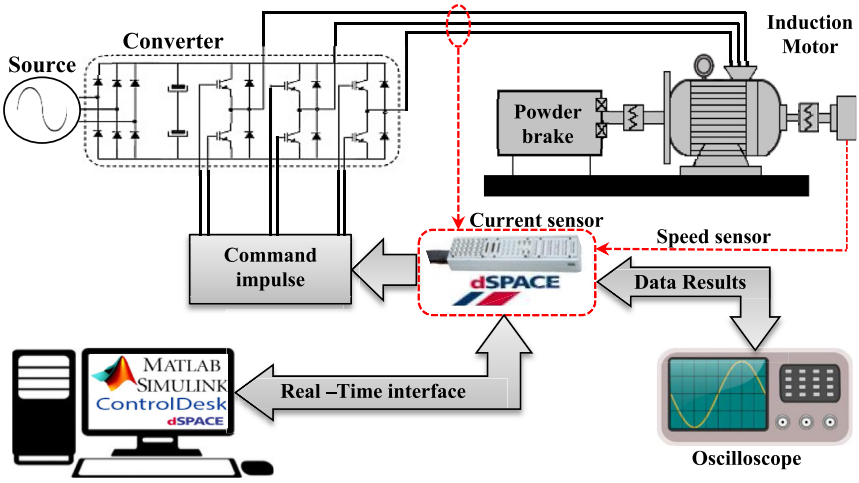

Fig. 10. Descriptive block diagram of the dSpace based experimental setup.

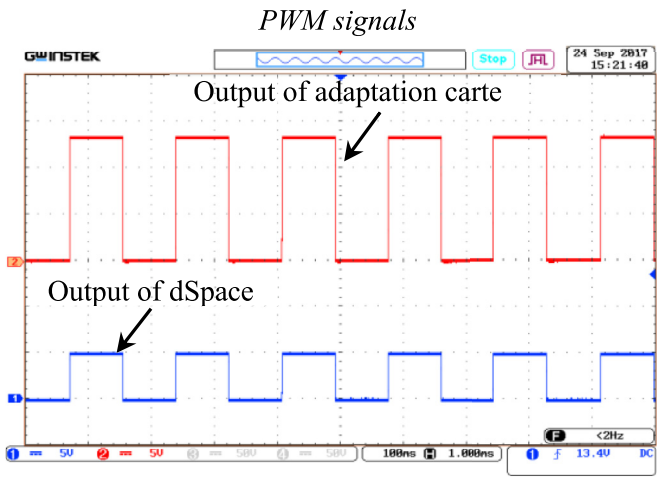

Fig. 11. PWM control signals.

$$S_i' = a_n + d_n + d_{(n-1)} + ...d_2 + d_1 \tag{12}$$

When the rotor bars fault appears in the IM, the wavelet can give information on the presence of the default. Whereas, the diagnosis is based on the observation and comparison between decomposition levels that contain the fault information. By calculating the associated eigenvalue with each level or each decomposition node, a highly efficient diagnostic tool can be constructed to evaluate the faults severity. The energy eigenvalue for each frequency band is defined by: [35]

$$E_j = \sum_{k=1}^{k=n} |D_{j,k}(n)|^2 \tag{13}$$

With j is the decomposition level, n is the DWT decomposition time, and D is the magnitude at each discrete point of the wavelet coefficient of the signal in the corresponding frequency band.

The energy eigenvalues of signals decomposition levels contain information which can be used for diagnosis process and the identification of fault's degree in the IM. The deviation of certain value indicates the severity of the failure.

5. Simulation results

The FOC control of the IM with rotor bars fault is simulated by using Matlab/Simulink software. The used motor in the simulation section is a 1.1 kW three phases squirrel cage with 16 rotor bars. The IM characteristics are given in the appendix. The global vector controlled IM based on the reduced model in healthy and faulty states are shown in Fig. 4.

The results of the vector controlled IM are given for healthy and faulty machines. When the speed is variable, the fault detection is considered by DWT analysis of the rotor speed, stator phase current and the output signal of the speed regulator. The fault severity is evaluated by the calculation of the stored energy in each level of the stator phase current, output signal of the speed regulator, and the active power. The used sampling frequency for the simulation section is 10 kHz.

5.1. Healthy state of the IM

Fig. 5 shows the simulation results of the electrical and mechanical quantities of the IM in healthy state. The test of the FOC will be achieved when the speed changes (the speed reference varies between 101 and 99 *rad/s* (≅ 964.478 and 945.380 rpm)) with rated load application during the launch of the IM.

For the variable speed operation in healthy state of the machine (Fig. 5), the rotor speed shows a good reference following and an accurate tracking without a static error. The electromagnetic torque and the stator phase currents show fast and good dynamics. Also, the direct and quadratic currents components are presented as an image of the rotor flux and electromagnetic torque respectively. The rotor flux components preserve a perfect decoupling between flux axes. Thereby, the results validate the proposed scheme.

5.2. Faulty state of the IM

In order to highlight the effect and the fault severity of the FOC control when the speed varies continuously, the broken rotor bars fault is simulated by increasing the bar resistance given in Eq. (3). In this case, the IM operates with nominal load and fault at the start-up.

By examining the results in Fig. 6, the broken rotor bars fault effect doesn't appear in the rotor speed and electromagnetic torque, due to the regulation of current and speed in the closed-loop which hides and compensates it. In contrast with a small oscillation appears in the stator phase current I_a, direct current I_{ds} and quadratic current I_{qs} respectively. However, the decoupling between the flux axes is preserved, therefore, it is noted that the FOC control is maintained robust vis-a-vis the fault.

5.3. Discrete wavelet analysis

To extract the fault components by using DWT, it's required to select the type of mother wavelet and the number of decomposition levels. The Daubechies-40 is used as the mother wavelet for the DWT analysis. The calculation of the decomposition level n depends on the sampling

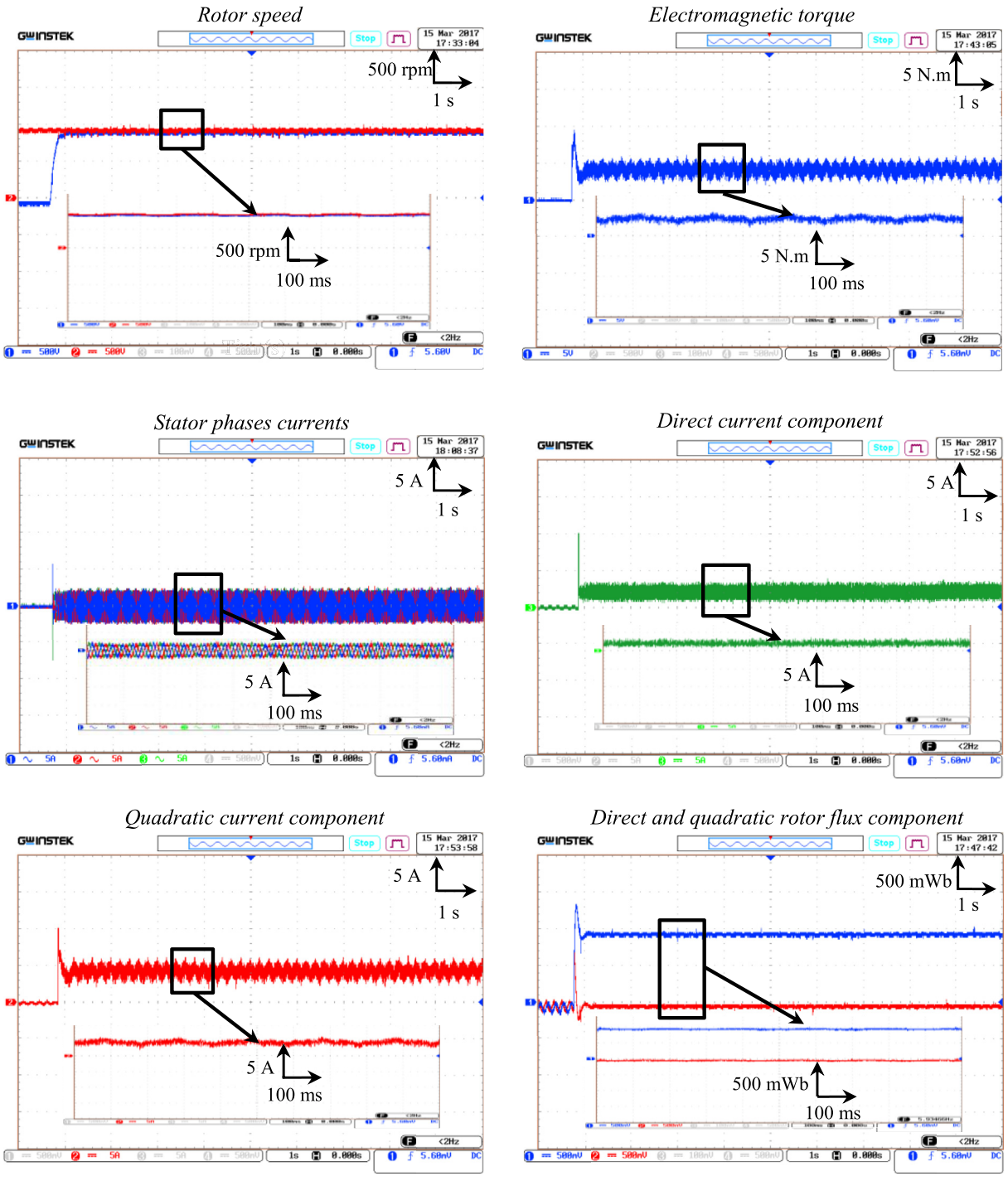

Fig. 12. Electrical and mechanical characteristic of the vector controlled IM in healthy state.

rate f_{sa} and the frequency net f_s. It can be obtained by using the following equation [15]:

$$n > \frac{\log(f_{sa}/f_s)}{\log(2)} + 1 \tag{14}$$

where:

The sampling rate was 10000 Hz and the supply frequency is 17.887 *Hz*.

Table 1 shows the frequency band for each level.

The rotor bars fault diagnosis based on spectrum analysis of sinusoidal current detects the sidebands harmonics around the fundamental supply frequency given by:

$$f_{rbb} = (1 \pm 2.n.\ s)f_s \tag{15}$$

where:

f_s is the frequency training of the machine, $s$is the slip and n = 1,2,3, ...

In the case of analyzing the non-sinusoidal (continuous) component, the harmonic frequency is given by:

$$f_{rbb} = 2.n.\ s.\ f_s \tag{16}$$

Table 2 shows the calculation frequencies of the broken rotor bars fault in simulation results of the stator phase current spectrums and the

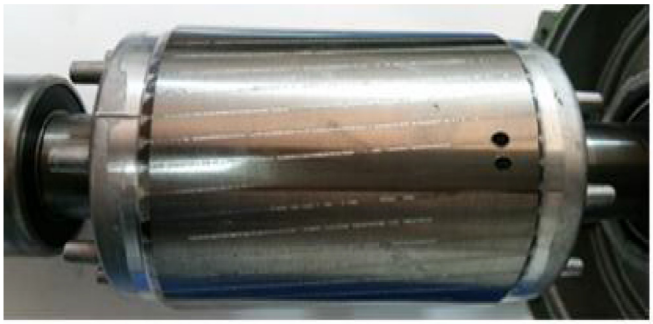

Fig. 13. Broken rotor bar of induction motor.

output signal of the speed regulator.

A medium speed value is considered in order to determine the medium slip and localize approximately the bands of the fault frequency. The application of the wavelet analysis permits to evaluate the fault when the speed is continually variable.

In Fig. 7, the DWT analysis of electrical and mechanical quantities are represented, where the same levels of decompositions (the a_{10}, d_{10}, d_9 and d_8 signals) are accounted in both results. The rotor bars fault identification in the rotor speed spectrum is very delicate due to the PI controller which maintains the regulation of the speed and corrects the fault influence. However, the analysis of the stator phase current shows a particular low variation at the d_{10}, d_9 and d_8 levels due to the fault, since they contain the frequency components $f_{rbb} = (1 \pm 2.n.s)f_s$ (Tables 1 and 2) compared to the healthy state of IM (Fig. 7a). Furthermore, the approximation a_{10} and the detailed d_{10} coefficients of the output signal of the speed regulator can be used for the fault detection, and it is manifested by oscillation which varies with the evolution of the frequency (Table 1 and Table 2).

The conspicuous problem for the fault diagnosis is when the rotor speed/reference changes continuously. Therefore, an important difference between signals level cannot be found in wavelet decomposition. The calculation of the stored energy in each level of signals is necessary in order to evaluate the severity of the fault.

Fig. 8 shows the simulation results of the stored energy for different levels of the stator phase current, the output signal of the speed regulator and the active power for healthy and faulty states of the machine.

When the fault occurs in the IM, the energy levels slightly increase in the stator phase current and the output signal of the speed regulator results (Fig. 8a and b), which fit the aforementioned characteristic. To overcome this problem, the calculation of the stored energy in each level of the active power is proposed in order to distinguish the fault effect. Therefore, it's remarked clearly in (Fig. 8c) that the active power signal's energy has increased by the fault. This result can be considered as an indicator of the rotor bars fault.

6. Experimental validation

The proposed control scheme with the diagnosis method will be verified also in experimental tests. The experimental results below illustrate the same conducted steps and tests as the simulation section. The same sampling frequency in the simulation tests is used for the real-time control; this value has been chosen with regard to the control scheme complexity. The experimental test bench has been realized in the laboratory of electrical engineering of Biskra (LGEB) from Algeria. The control algorithm is implemented using dSpace DS1104 R&D controller board with control desk and Matlab/Simulink software package. Fig. 9 shows the experimental ground of IM drive which is essentially composed of *1.1 kW* squirrel-cages IM (healthy and faulty states) driven by a SEMIKRON converter that is composed of a rectifier and IGBT inverter. A magnetic powder brake is used as load is coupled to the rotor of IM, and an incremental encoder used as a speed sensor and as well as position sensor. The currents and voltages, respectively, are sensed by current (Hall-type) and voltage sensors. Then, an auto-transformer *(0-450V)* linked to the grid is used for power supply.

Fig. 10 shows the descriptive diagram of experimental setup and software/hardware linkage. The execution of the program inside the DSP of dS1104 board converts it into a real-time system on the hardware (dSpace 1104 RTI) after it was in the software (Simulink). In addition, the Control Desk visual interface gives us the access to adjust all Simulink variables in real-time in order to obtain a satisfied control behavior. The PWM switching sequences are calculated in Matlab/Simulink with a commutation frequency equal to *5 kHz*, then, they are generated by an analog digital converter using dSpace interface board. In order to control the IGBT grid and increase noise immunity, the control signals are maintained in the analog format with (*0–5 V*) voltage, and they are offset from one another. The delivered dSpace output signals (PWM) will be amplified to (*0–15 V*) by an adaptation carte which was carried out in the laboratory (Fig. 11). A supply voltage of (400 V) is filtered through the rectifier in order to fix the DC-bus of the converter. After that, the dS1104 receives another time the input signals by currents sensor from (ADC) ports and speed from encoder through (INC) ports. Finally, the IM has been controlled via Control Desk, where the results were obtained by a numerical oscilloscope (GW-INSTEK) which was plugged with the real-time interface through (DAC) ports.

Remark 1. The used induction machines in the experimental implementation have different characteristics with the used machine in simulation section, but they preserve the same power *(1,1* kW*)*. The reduced rotor cage model identification is more complex than the classical model and requires specified information about machine geometry in which, unfortunately, they can be offered only by the constructor; for this reason, we have used in this work another machine with an equivalent characteristic. It can be confirmed that this mismatch between two machines didn't confuse the studied phenomena which already have been analyzed by simulation tests.

6.1. 1 Healthy state of the IM

The figures below show the experimental results of the vector controlled IM in healthy state. Several electrical and mechanical quantities of the IM at measured time of *10s* with zoom effected at *1s* are presented, in order to compare with simulation results.

Fig. 12 illustrates the experimental results of the FOC control of the IM in healthy state, the load is applied at start-up. It is noted that the rotor speed response presents a full superposition without overshoot (1div = 500 rpm). This indicates to the good tracking as observed in ZOOM of rotor speed. The electromagnetic torque (1div = 5 N m) shows fast dynamic. The waveform of the stator phase currents is correctly sinusoidal (1div = 5 A). The direct current component (1div = 5A) is stabilized in the rated value, while the quadratic current component (1div = 5A) follows perfectly the torque evolution. The rotor flux components (1div = 0.5 Wb) show a good orientation with a perfect decoupling.

6.2. 2 Faulty state of the IM

In experimental tests, the broken rotor bars fault has been realized by drilling a small hole of 3.1 mm diameter in all the rotor bar depth as shown in Fig. 13.

The FOC is carried out in faulty state of the operating machine with variable reference speed of 101 to 99 rad/s (≅ 964.478 to 945.380 rpm) and the load is applied at the start-up.

The analysis of the obtained results in faulty state (Fig. 14) by comparison to the healthy state (Fig. 12), shows that the rotor speed and electromagnetic torque are not affected by the broken rotor bars fault owing to closed-loop control. However, the amplitude of stator

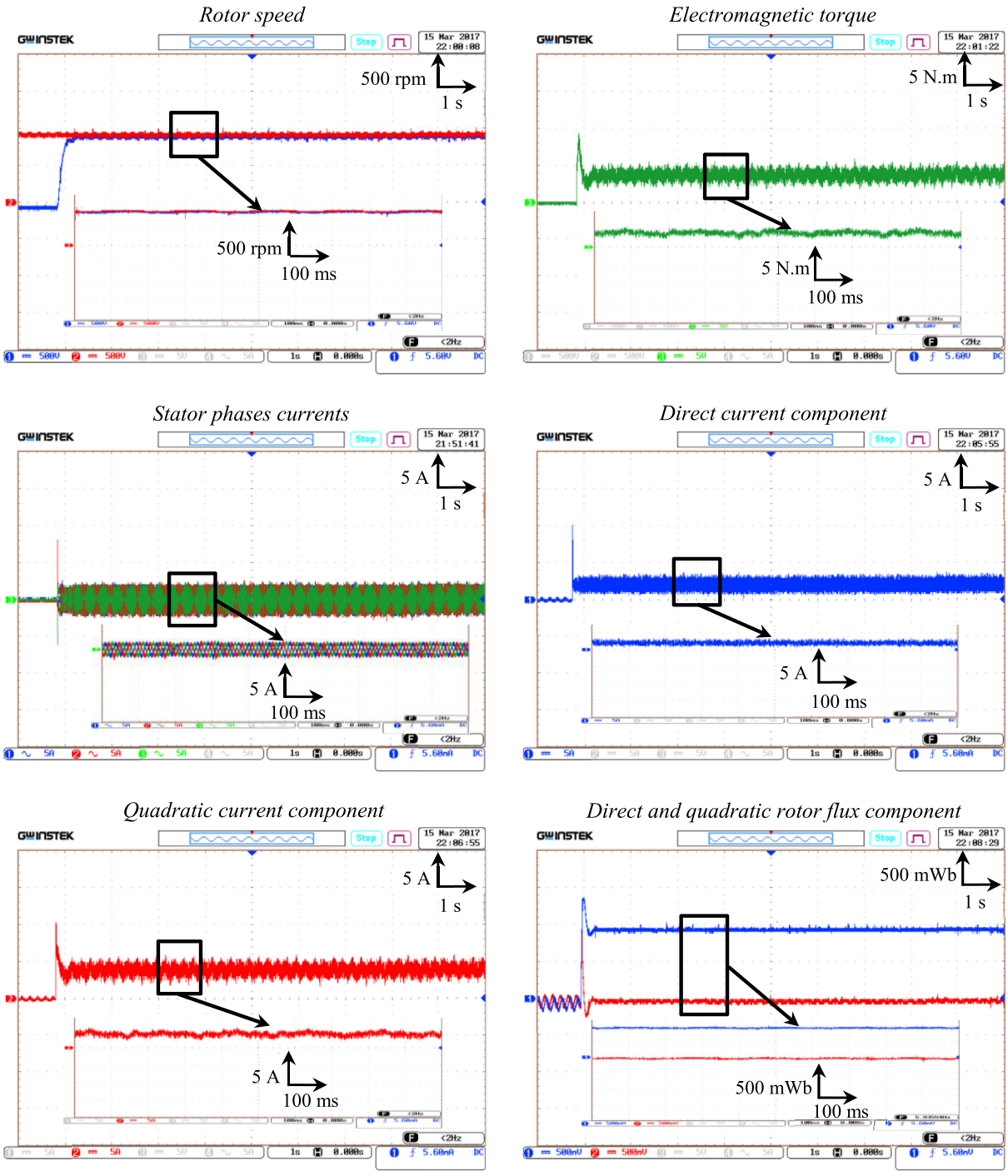

Fig. 14. Electrical and mechanical characteristic of the vector controlled IM in faulty state.

phase current isn't constant; a perturbation provoked by the fault is observed in the direct and quadratic current components.

Briefly, the experimental and the simulation results give the same phenomena in the faulty state of the machine when the speed varies continuously.

6.3. 3 DWT signals analysis

The DWT has been used also for the rotor bars fault diagnosis of the IM in experimental tests. The decomposition levels n will be calculated by using Eq. (13), where, the sampling rate was 10000 Hz and the supply frequency is 36.042 Hz in the real-time implementation.

Table 3
Frequency Levels of Wavelet Coefficients in experimental tests.

Level	Frequency band
d_1	2500–5000 Hz
d_2	1250–2500 Hz
d_3	625–1250 Hz
d_4	312.5–625 Hz
d_5	156.25–312.5 Hz
d_6	78.12–156.25 Hz
d_7	39.06–78.12 Hz
d_8	19.53–39.06 Hz
d_9	9.76–19.53 Hz
a_9	0–9.76 Hz

Table 4
Frequencies of the stator current and the output signal of the speed regulator with fault in experimental tests.

stator phase current I_a spectrum					quadratic current I_{qs} spectrum		
$s = 0.1169$	$(1\text{-}2s)f_s$	$(1\text{-}4s)f_s$	$(1+2s)f_s$	$(1+4s)f_s$	$s = 0.1169$	$2sf$	$4sf$
$f_{calculated}$ (Hz)	27.619	19.169	44.466	52.896	$f_{calculated}$ (Hz)	8.423	16.853

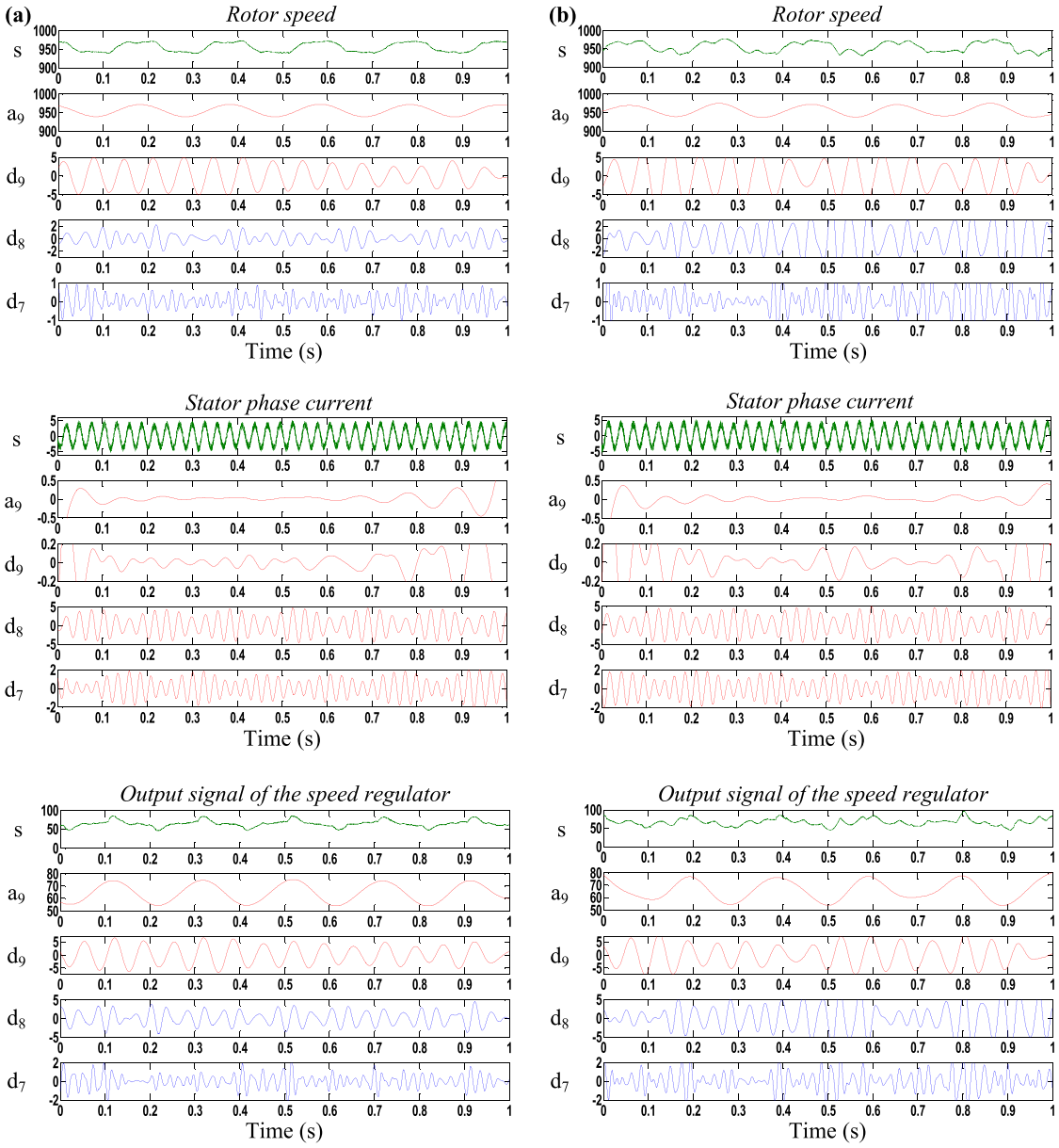

Fig. 15. DWT of the rotor speed, the stator phase current and the output signal of the speed regulator.

Table 3 presents the frequency band for each decomposition level.

Table 4 illustrates the calculation frequencies of the rotor bars fault in experimental results of the stator phase current aw well as in the output signal of the speed regulator.

Fig. 15 shows the DWT analysis in experimental results of the rotor speed, the stator phase current, and the output signal of the speed regulator in healthy and faulty states of the IM. The rotor speed analysis using DWT is very difficult to distinguish between the fault and the healthy state, since the same signal has appeared in the a_9 level. As we have mentioned before, the control-loop masks and compensates the fault effect. For this reason, the analysis of the output signal of the speed regulator is proposed to solve this problem.

However, the comparison between the results of DWT analysis of stator phase current and the output signal of the speed regulator in healthy state (Fig. 15a) and faulty state (Fig. 15b) can be summarized in the following points:

- An oscillation and small variation is shown in both results,
- The amplitude coefficient levels a_9, d_9, d_8 and d_7 for the stator current and a_9, d_9 for the output signal of the speed regulator are increased.

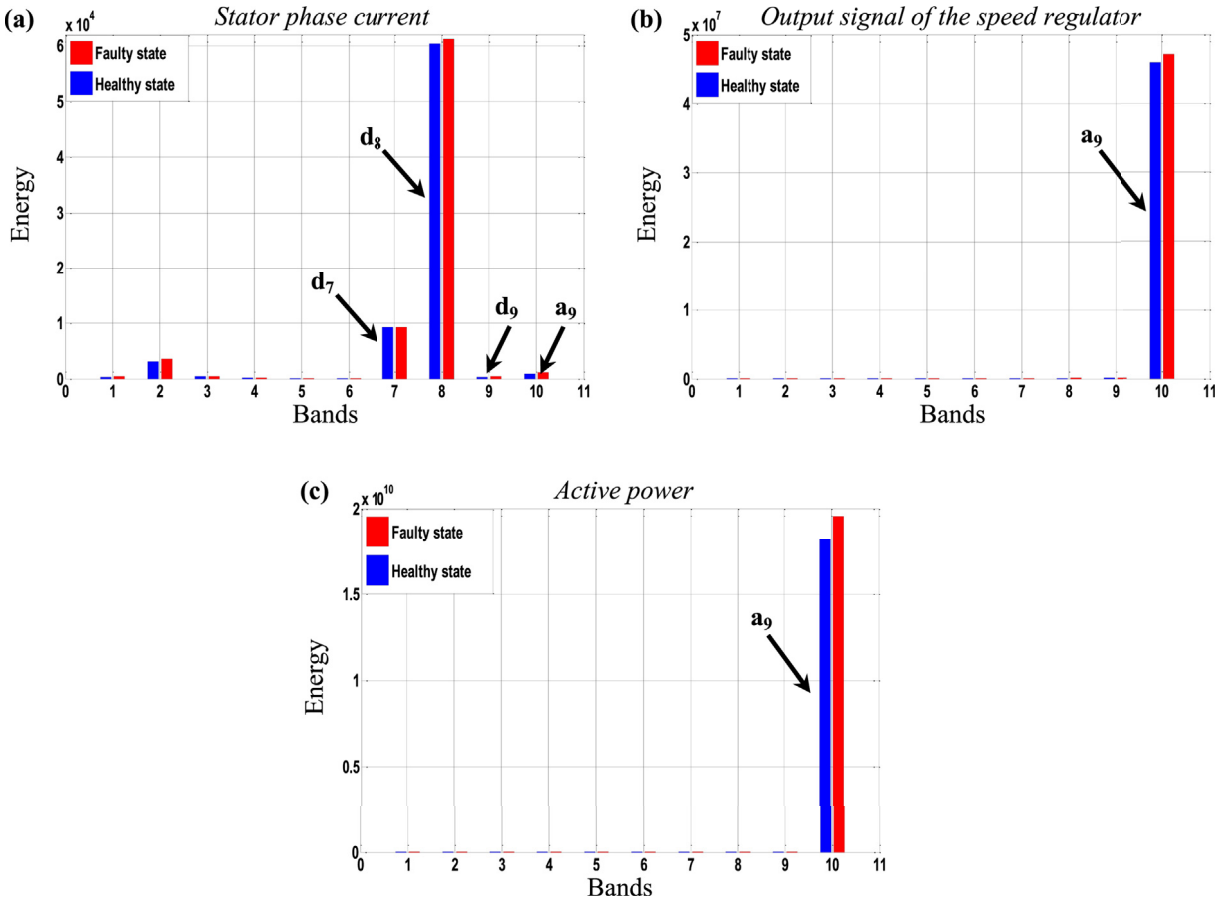

Fig. 16. Energy value for various levels:(a) Stator phase current, (b) Output signal of the speed regulator and (c) Active power.

The DWT analysis obtained for the experimental results are similar with the simulation results. The direct analysis obtained by DWT is very difficult to view the severity of the fault in signals level. For this, the energy stored in each level of DWT is necessary (Fig. 16).

Fig. 16 shows the stored energy value for the experimental results of the stator phase current, the output signal of the speed regulator, and the active power respectively. In comparison to the faulty and the healthy states of the machine, a small increase of the energy value is observed for the stator current (Fig. 16a) and the output signal of the speed regulator (Fig. 16b). Contrariwise, a considerable increase of the proposed energy for the active power (Fig. 16c), this result can be used as a good indicator for the fault detection and for the fault severity.

7. Conclusion

In variable speed drives, the fault detection and diagnosis are very delicate. For this issue, a simulation and an experimental study are considered for the machine in closed-loop drives using a FOC technique. A reduced model for the rotor cage, with taking into account the rotor bars fault of the IM, has been used for the control design. The vector control is introduced as IM variable speed drive, particularly, when the speed varies continuously and the machine operates with rotor bars fault. The obtained simulation and experimental results give a high robustness against the fault effect and a good control performance like an accurate reference tracking and fast response.

For the diagnosis purpose, the DWT has been employed to analyze several electrical and mechanical control quantities when the machine operates with continuously variable speed.

The DWT analysis of the stator phase current and the output signal of the speed regulator don't show clearly the fault effect. The calculation of the stored energy in each decomposition levels gives information about the broken rotor bars fault, particularly for the active power energy. This information can be used for the determination and the severity of the fault when the machine operates with variable speed. The result is evaluated in simulation and confirmed by the experimental results.

Nomenclature

IM	Induction machine
FOC	Field oriented control
DWT	Discrete Wavelet Transform
RTI	Real-Time interface
Vdc	Direct voltage
V_a, V_b, V_c	Three phases reference voltages *a, b, c*
S_a, S_b, S_c	Switching states of the inverter *a, b, c*
V_{dsref}, V_{qsref}	*(d,q)* axis reference voltages of the stator
I_a, I_b, I_c	Three phases currents *a, b, c* of the stator
I_{ds}, I_{qs}	*(d,q)* axis current components of the stator

$_{Ie}$	Short circuit ring current
$_{[I]}$	Current vector
$_{[L]}$	Inductance matrix
$_{[R]}$	Resistance matrix
$_{[V]}$	Voltage vector
R_{bfk}	Resistance of the bar index k
x	State variable
u	Control variable
y	Measurable output
N_r	Number of rotor bars
e	Air-gap mean diameter
l	Active length of the magnetic circuit
R	Average radius of the air gap
μ_0	Magnetic permeability of the air
α	Angle between two broken rotor bars
$_s$	Motor slip
PI	Proportional-Integrator
ω_r	Electrical rotor speed in rad/s
T_e	Electromagnetic torque

Appendix

IM used in the simulation results.

P_n	Output power	1.1 kW
V_s	Stator voltage	400/230 V
I_s	Nominal current	2.5/4.3A
p	Number of Pole pairs	1
R_s	Stator resistance	7.58Ω
R_r	Rotor resistance	6.3 Ω
R_b	Rotor bar resistance	0.15 mΩ
R_e	Resistance of end ring segment	0.15 mΩ
L_b	Rotor bar inductance	0.1 μH
L_e	Inductance of end ring	0.1 μH
L_{sf}	leakage inductance of stator	26.5 mH
M_{sr}	Mutual inductance	46.42 mH
N_s	Number of turns per stator phase	160
N_r	Number of rotor bars	16
e	Air-gap mean diameter	2.5 mm
l	Active length of the magnetic circuit	65 mm
R	Average radius of the air gap	35.7 mm
J	Inertia moment	0.0054 kg m^2
F	Coefficient of damping	0.00119 N.m/rad/s

IM used in the experimental results.

P_n	Output power	1.1 kW
V_s	Stator voltage	400/230 V
I_s	Nominal current	2.5/4.3A
p	Number of Pole pairs	2
R_s	Stator resistance	6.75Ω
R_r	Rotor resistance	6.21Ω
L_s	Stator inductance	0.5192H
L_r	Rotor inductance	0.5192H
M_{sr}	Mutual inductance	0.4957H
N_r	Number of rotor bars	46
J	Inertia moment	0.0124 kg.m2
F	Coefficient of damping	0.0029 N.m/rad/s

References

[1] Bachir S, Tnani S, Trigeassou JC, Champenois G. Diagnosis by parameter estimation of stator and rotor faults occurring in induction machines. IEEE Trans Ind Electron 2006;53:963–73. http://dx.doi.org/10.1109/TIE.2006.874258.

[2] Guezmil A, Berriri H, Pusca R, Sakly A, Romary R, Mimouni MF. Detecting inter-turn short-circuit fault in induction machine using high-order sliding mode observer: simulation and experimental verification. J Control Autom Electr Syst 2017. http://dx.doi.org/10.1007/s40313-017-0314-2.

[3] Rajalakshmi Samaga BL, Vittal KP. Comprehensive study of mixed eccentricity fault diagnosis in induction motors using signature analysis. Int J Electr Power Energy Syst 2012;35:180–5. http://dx.doi.org/10.1016/j.ijepes.2011.10.011.

[4] Talhaoui H, Menacer A, Kechida R. Mixed eccentricity fault diagnosis in the sensorless field oriented control induction motor using DWT technique. Diagnostics Electr Mach power Electron drives (SDEMPED), 2015 IEEE 10th Int symp 2015. p. 97–103. http://dx.doi.org/10.1109/DEMPED.2015.7303675.

[5] Moussa MA, Boucherma M, Khezzar A. A detection method for induction motor bar fault using sidelobes leakage phenomenon of the sliding DFT. IEEE Trans Power Electron 2016:1–13. http://dx.doi.org/10.1109/TPEL.2016.2605821.

[6] Bessam B, Menacer A, Boumehraz M, Cherif H. Detection of broken rotor bar faults in induction motor at low load using neural network. ISA Trans 2016:1–6. http://dx.doi.org/10.1016/j.isatra.2016.06.004.

[7] Menacer A, Moreau S, Benakcha A, Said MSN. Effect of the position and the number of broken bars on asynchronous motor stator current spectrum. 2006 12th int. Power electron. Motion control conf. IEEE; 2006. p. 973–8. http://dx.doi.org/10.1109/EPEPEMC.2006.4778526.

[8] Nandi S, Toliyat HA. Condition monitoring and fault diagnosis of electrical machines-a review. Conf. Rec. 1999 IEEE ind. Appl. Conf. Thirty-forth IAS annu. Meet. (Cat. No.99CH36370), vol. 1. IEEE; 2005. p. 197–204. http://dx.doi.org/10.1109/IAS.1999.799956.

[9] Casadei D, Profumo F, Tani A. FOC and DTC: two viable schemes for induction motors torque control. IEEE Trans Power Electron 2002;17:779–87. http://dx.doi.org/10.1109/TPEL.2002.802183.

[10] Ameid T, Menacer A, Talhaoui H, Harzelli I. Broken rotor bar fault diagnosis using fast Fourier transform applied to field-oriented control induction machine: simulation and experimental study. Int J Adv Manuf Technol 2017. http://dx.doi.org/10.1007/s00170-017-0143-2.

[11] El Hachemi Benbouzid M. A review of induction motors signature analysis as a medium for faults detection. IEEE Trans Ind Electron 2000;47:984–93. http://dx.doi.org/10.1109/41.873206.

[12] Chen K, Huang C, He J. Fault detection, classification and location for transmission lines and distribution systems: a review on the methods. High Volt 2016;1:25–33. http://dx.doi.org/10.1049/hve.2016.0005.

[13] Ramana DV, Baskar S. Diverse fault detection techniques of three-phase induction motor — a review. 2016. Int. Conf. Emerg. Technol. Trends IEEE; 2016. p. 1–8. http://dx.doi.org/10.1109/ICETT.2016.7873779.

[14] Talhaoui H, Menacer A, Kessal A, Kechida R. Fast Fourier and discrete wavelet transforms applied to sensorless vector control induction motor for rotor bar faults diagnosis. ISA Trans 2014;53:1639–49. http://dx.doi.org/10.1016/j.isatra.2014.06.003.

[15] Kechida R, Menacer A, Benakcha A. fault detection of broken rotor bars using stator current spectrum for the direct torque control induction motor. World Acad Sci Eng Technol 2010;4:1230–5.

[16] Saidi L, Fnaiech F, Henao H, Capolino GA, Cirrincione G. Diagnosis of broken-bars fault in induction machines using higher order spectral analysis. ISA Trans 2013;52:140–8. http://dx.doi.org/10.1016/j.isatra.2012.08.003.

[17] Menacer A, Kechida R, Champenois G, Tnani S. Application of the Fourier and the wavelet transform for the fault detection in induction motors at the startup electromagnetic torque. SDEMPED 2011-8th IEEE symp diagnostics electr mach power electron drives 2011. p. 664–8. http://dx.doi.org/10.1109/DEMPED.2011.6063695.

[18] Bouzida A, Touhami O, Ibtiouen R, Belouchrani A, Fadel M, Rezzoug a. Fault diagnosis in industrial induction machines through discrete wavelet transform. IEEE Trans Ind Electron 2011;58:4385–95. http://dx.doi.org/10.1109/TIE.2010.2095391.

[19] da Costa C, Kashiwagi M, Mathias MH. Rotor failure detection of induction motors by wavelet transform and Fourier transform in non-stationary condition. Case Stud Mech Syst Signal Process 2015;1:15–26. http://dx.doi.org/10.1016/j.csmssp.2015.05.001.

[20] Antonino-Daviu J, Riera-Guasp M, Pons-Llinares J, Park J, Bin Lee S, Yoo J, et al. Detection of broken outer-cage bars for double-cage induction motors under the startup transient. IEEE Trans Ind Appl 2012;48:1539–48. http://dx.doi.org/10.1109/TIA.2012.2210173.

[21] Panigrahy PS, Konar P, Chattopadhyay P. Broken bar fault detection using fused DWT-FFT in FPGA platform. 2014 Int conf power, control embed syst ICPCES 2014 2014. http://dx.doi.org/10.1109/ICPCES.2014.7062819.

[22] Briz F, Degner MW, García P, Bragado D. Broken rotor bar detection in line-fed induction machines using complex wavelet analysis of startup transients. Conf Rec - IAS Annu Meet (IEEE Ind Appl Soc 2007;44:2254–61. http://dx.doi.org/10.1109/IAS.2007.341.

[23] Cherif H, Menacer A, Bessam B, Kechida R. Stator inter turns fault detection using discrete wavelet transform. 2015 IEEE 10th int. Symp. Diagnostics electr. Mach. Power electron. Drives, vol. 55. IEEE; 2015. p. 138–42. http://dx.doi.org/10.1109/DEMPED.2015.7303681.

[24] Shi Pu, Chen Zheng, Vagapov Y, Davydova A, Lupin S. Broken bar fault diagnosis for induction machines under load variation condition using discrete wavelet transform. Proc. IEEE east-west des. Test symp. (EWDTS 2014) IEEE; 2014. p. 1–4. http://dx.doi.org/10.1109/EWDTS.2014.7027059.

[25] Kia SH, Henao H, Capolino G-A. Diagnosis of Broken-bar fault in induction machines using discrete wavelet transform without slip estimation. IEEE Trans Ind Appl 2009;45:1395–404. http://dx.doi.org/10.1109/TIA.2009.2018975.

[26] Kechida R, Menacer A, Talhaoui H. Approach signal for rotor fault detection in induction motors. J Fail Anal Prev 2013;13:346–52. http://dx.doi.org/10.1007/s11668-013-9681-6.

[27] Bellini A, Concari C, Franceschini G, Tassoni C. Different procedures for the diagnosis of rotor fault in closed loop induction motors drives. Proc IEEE int electr mach drives conf IEMDC 2007, vol. 2. 2007. p. 1427–33. http://dx.doi.org/10.1109/IEMDC.2007.383638.

[28] Serna E, Pacas JM. detection of Rotor fault in field oriented controlled induction machines. Proc 41st IAS Annu Meet Ind Appl Conf Tampa n.d. http://dx.doi.org/10.1109/IAS.2006.256866.

[29] Singh A, Grant B, Defour R, Sharma C, Bahadoorsingh S. A review of induction motor fault modeling. Electr Power Syst Res 2016;133:191–7. http://dx.doi.org/10.1016/j.epsr.2015.12.017.

[30] Menacer A, T-Said M d N, Benakcha A, Drid S. Stator current analysis of incipient fault into asynchronous motor rotor bars using fourier fast transform. J Electr Eng 2004;55:122–30.

[31] Ameid T, Menacer A, Talhaoui H, Harzelli I, Ammar A. Simulation and real-time implementation of sensorless field oriented control of induction motor at healthy state using rotor cage model and EKF. 2016 8th Int. Conf. Model. Identif. Control IEEE; 2016. p. 695–700. http://dx.doi.org/10.1109/ICMIC.2016.7804201.

[32] Zhu KP, Wong YS, Hong GS. Wavelet analysis of sensor signals for tool condition monitoring: a review and some new results. Int J Mach Tools Manuf 2009;49:537–53. http://dx.doi.org/10.1016/j.ijmachtools.2009.02.003.

[33] Vitor ALO, Scalassara PR, Endo W, Goedtel A. Induction motor fault diagnosis using wavelets and coordinate transformations. 2016 12th IEEE Int. Conf. Ind. Appl. INDUSCON 2016 2017. http://dx.doi.org/10.1109/INDUSCON.2016.7874502.

[34] Yahia K, Cardoso AJM, Ghoggal A, Zouzou SE. Induction motors airgap-eccentricity detection through the discrete wavelet transform of the apparent power signal under non-stationary operating conditions. ISA Trans 2014;53:603–11. http://dx.doi.org/10.1016/j.isatra.2013.12.002.

[35] Kapoor SR, Khandelwal N, Pareek P. Bearing fault analysis by signal energy calculation based signal processing technique in Squirrel Cage Induction Motor. 2014 Int. Conf. Signal propag. Comput. Technol. (ICSPCT 2014) IEEE; 2014. p. 33–8. http://dx.doi.org/10.1109/ICSPCT.2014.6884922.